ELSEVIER

Quaternary Science Reviews 26 (2007) 2644–2660

QSR

High-altitude varve records of abrupt environmental changes and mining activity over the last 4000 years in the Western French Alps (Lake Bramant, Grandes Rousses Massif)

Hervé Guyard[a,b,c,*], Emmanuel Chapron[d], Guillaume St-Onge[b,c], Flavio S. Anselmetti[d], Fabien Arnaud[e], Olivier Magand[f], Pierre Francus[g,c], Marie-Antoinette Mélières[f,h]

[a]*Université Bordeaux 1, DGO, UMR EPOC 5805, Avenue des facultés, 33405 Talence Cedex, France*
[b]*Institut des sciences de la mer de Rimouski (ISMER), Université du Québec à Rimouski, 310 allée des Ursulines, Rimouski, Québec Canada, G5L 3AI*
[c]*Centre de recherche en géochimie et géodynamique (GÉOTOP-UQÀM-McGill), Université du Québec à Montréal, C.P. 8888, Succ. Centre-Ville, Montréal, Québec Canada, H3C 3P8*
[d]*Geological Institute ETH Zürich, Universitätstrasse 16, CH-8092 Zürich, Switzerland*
[e]*Laboratoire EDYTEM, UMR 5204, Université de Savoie, F-73376 Le Bourget du Lac, France*
[f]*Laboratoire de Glaciologie et de Géophysique de l'Environnement (LGGE), CNRS, Université Joseph Fourier Grenoble, Domaine Universitaire BP 36, F-38402 Saint Martin d'Hères, France*
[g]*Institut National de la Recherche Scientifique- Eau, Terre, et Environnement (INRS-ETE), Québec Canada, G1K 9A9*
[h]*Institut de la Montagne, Université de Savoie, F-73376 Le Bourget du Lac, France*

Received 1 February 2007; received in revised form 10 July 2007; accepted 11 July 2007

Abstract

Two twin short gravity cores and a long piston core recovered from the deepest part of proglacial Lake Bramant (Grandes Rousses Massif, French Alps), under and overlying a large slump identified by high-resolution seismic profile, allow the investigation of Holocene natural hazards and interactions between human activity and climatic changes at high-altitude. Annual sedimentation throughout the cores (glacial varves) is identified on photographs, ITRAX (high-resolution continuous microfluorescence-X) and CAT-Scan (computerized axial tomography) analyses and is supported by (1) the number of dark and light laminations between dates obtained by radionuclide measurements (^{137}Cs, ^{241}Am), (2) the correlation of a slump triggered by the nearby AD 1881 Allemond earthquake (MSK intensity VII) and of a turbidite triggered by the AD 1822 Chautagne regional earthquake (MSK intensity VIII), (3) the number of laminations between two accelerator mass spectrometry (AMS) ^{14}C dates, and (4) archaeological data. In Lake Bramant, dark layers are coarser, contain less detrital elements, but more neoformed elements and organic matter content. These darker laminations result from calm background sedimentation, whereas the lighter layers are finer and rich in detrital elements and reflect the summer snowmelt. Traces of mining activity during the Roman civilization apogee (AD 115–330) and during the Early Bronze Age (3770–3870 cal BP) are recorded by lead and copper content in the sediments and probably result from regional and local mining activity in the NW Alps. Warmer climate during the Bronze Age in this part of the Alps is suggested by (1) two organic deposits (4160–3600 cal BP and 3300–2850 cal BP) likely reflecting a lower lake level and smaller glaciers and (2) evidence of a different vegetation cover around 2500 m a.s.l. The onset of clastic proglacial sedimentation between 3600–3300 cal BP and since 2850 cal BP is synchronous with periods of glacier advances documented in the Alps and high-lake levels in west-central Europe. This major change in proglacial sedimentation highlights the development of a larger St. Sorlin glacier in the catchment area of Lake Bramant.

1. Introduction

High-altitude lakes are often used as archives for past environmental changes and mountain glaciers are valuable tools to investigate climate variability over decadal to

*Corresponding author. Institut des sciences de la mer de Rimouski (ISMER, UQAR), 310, allée des Ursulines, Rimouski (Qc) Canada G5L3A1. Tel.: +1 418 723 1986 x 1230; fax: +1 418 724 1842.
E-mail address: herve.guyard@uqar.qc.ca (H. Guyard).

0277-3791/$ - see front matter © 2007 Elsevier Ltd. All rights reserved.
doi:10.1016/j.quascirev.2007.07.007

centennial timescale (Leeman and Niessen, 1994; Leonard, 1997; Intergovernmental Panel on Climate Change (IPCC), 2001; Blass et al., 2003; Deline and Orombelli, 2005; Holzhauzer et al., 2005). Millennial to centennial-scale Holocene climatic oscillations in the Alps and surrounding regions have been documented by lake-level changes, archaeological evidence and palynological records from many small lakes in the Jura Mountains and several larger lakes in the NW French Alps and in the Swiss Plateau (see Magny et al., 2003; Magny, 2004; Holzhauzer et al., 2005 for a review). Within radiocarbon dating uncertainties, cold and wet periods favouring high lake levels seem to coincide with well-documented advances of Swiss and Austrian glaciers and with tree-line descent in the Central and Southern Alps. In the French Western Alps, Holocene glacier fluctuations are documented in the Mont Blanc Massif by few radiocarbon-dated glacial or fluvio-glacial deposits and by a well-dated continuous record of flooding activity from a large lake downstream of these glaciers (see Chapron et al., 2002, 2005; Arnaud et al., 2005a, b for a review). Since 2800 cal BP, however, increasing land use in Alpine valleys is interacting with climate and influences environmental changes and clastic lacustrine sedimentation (Noël et al., 2001; Arnaud et al., 2005a, b). In contrast to these alpine valleys, little is known about the evolution of human activities in high-altitude alpine catchment areas and their interactions with environmental changes.

Over the last decades, several studies have demonstrated in various arctic and alpine environments that proglacial lakes can provide continuous high-resolution sedimentary records of glacial activity in their catchment (Matthews and Karlén, 1992; Leeman and Niessen, 1994; Ariztegui et al., 1997; Leonard, 1997; Nesje et al., 2000; Blass et al., 2003; Dahl et al., 2003; Tomkins and Lamoureux, 2005; Lamoureux et al., 2006; Anselmetti et al., 2007). Because bedrock erosion rate increases with glacier size and thickness, variations through time in the accumulated amount of silt- and clay-sized mineral fraction in proglacial lake sediments provide a reliable record of glacier activity and thus, of climate changes. Furthermore, studies in the Alpine region have shown that lacustrine sedimentation can also provide detailed record of regional seismo-tectonic activities (Chapron et al., 1999; Arnaud et al., 2002; Schnellmann et al., 2002; Monecke et al., 2004; Nomade et al., 2005; Strasser et al., 2006) or of metallic contaminations related to mining activities since the Roman period (Shotyk and Krachler, 2004; Arnaud et al., 2005a, b).

This paper presents the first results of a multidisciplinary study of the sedimentary infill of proglacial Lake Bramant, the lowest in a chain of three proglacial lakes in the

Table 1
Evolution of human activities in the Grandes Rousses Massif over the last 4000 years

Chronological period	Age (BC/AD)	Age (cal BP)	Human activities in the Massif
Modern period	AD 1918–present		Hydroelectric dam construction, tourism
Middle Age	476–1492 AD	1474–458	Mining industry, pasturing
Roman period	50 BC–476 AD	2000–1474	Pasturing, deforestation
Iron Age	750–50 BC	2700–2000	Unknown
Late Bronze Age	1400–750 BC	3300–2700	Unknown
Middle Bronze Age	1700–1350 BC	3600–3300	Unknown
Early Bronze Age	2300–1650 BC	4250–3600	Mining industry

The chronological limits of the periods are those retained by the *Service Régional de l'Archéologie*.

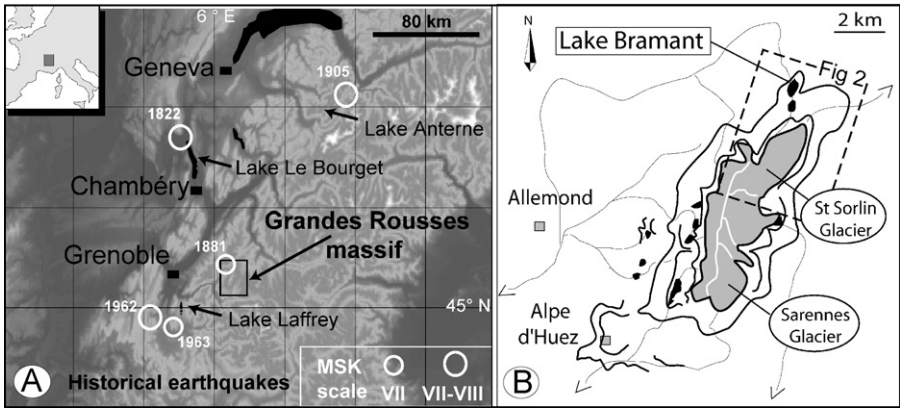

Fig. 1. General location of the Grandes Rousses massif in the French Alps (A) and of Lake Bramant in the north of this massif (B). Also shown are the MSK intensities at the epicentres of regional historical earthquakes previously recorded in lake sediments as discussed in the text. The Grandes Rousses massif is characterized by several belts of frontal moraines and cirque glaciers draining into proglacial lakes. The St. Sorlin and Sarennes glaciers are instrumented since several decades and considered as representative for the NW Alps.

northern part of the Grandes Rousses Massif (Western Alps, France, Fig. 1). A precise chronostratigraphy in this high-altitude lake is established based on glacial varve counting, radionuclide measurements and radiocarbon dating. It allows especially the correlation of a major mass wasting deposit with a strong local earthquake and it relates atmospheric metallic contaminations to mining activities in this part of the Alps. Important changes in proglacial sedimentation during the Middle Bronze Age and since the end of the Late Bronze Age (Table 1) are used to document environmental changes in relation with glacier fluctuations in the drainage basin, lake level changes and human activities in this alpine region.

2. Setting

The Grandes Rousses Massif (45°7′N, 6°6′E) is characterized by glaciers located between 3400 and 2500 m a.s.l., and by the occurrence of up to five generations of moraine belts formed below the present-day glacier snout positions. Two glaciers located on the southern (Sarennes) and northern (St. Sorlin) side of the massif (Fig. 1b) have been instrumented since 1949 and 1957, respectively, and are generally considered as representative for the NW Alpine region (Six et al., 2001; Torinesi et al., 2002; Vincent, 2002). Several proglacial lakes are located below the uppermost moraine belt resulting from the last advance of glaciers during the "Little Ice Age" (LIA) in AD 1820–1850 (Fuselin et al., 1909; Allix, 1927; Edouard, 1994).

St. Sorlin glacier (Fig. 2) is a small glacier (3 km^2), but the largest of the Grandes Rousses Massif. It is exposed to the North and collects most of the precipitation falling in a cirque of ca. 5 km^2 lying entirely above 2700 m a.s.l. (Lliboutry, 2002). St. Sorlin glacier mass-balance calculations (Vincent, 2002) and an ice-flow model (Le Meur and Vincent, 2003) covering the period between 1907 and 1999 were based on direct glaciological measurements, on aerial photographs, and on a first geomorphologic map made in 1907 (Fuselin et al., 1909). This glacier forms a diffluence on a bedrock knob near the location of the alpine hut at 2710 m a.s.l., used as a base camp during glaciological studies (Fig. 2). Because of this diffluence, only the western part of St. Sorlin glacier (contoured in Fig. 2) belongs to the drainage basin of a chain of three small proglacial lakes (lakes Tournant, Blanc Bramant and Bramant) that are aligned in the so-called Bramant Valley. These lakes of glacial origin are dammed by three generations of frontal moraines formed after the Younger Dryas according to geomorphologic correlations (Fuselin et al., 1909; Edouard, 1994) and pollen studies in the south of the massif (Chardon, 1991).

Glacial erosion of the bedrock (consisting of gneiss, schist, Carboniferous and Triassic sedimentary rocks) in this small glacial valley has been enhanced by the development of intense NS and NW–SE faulting during the formation of the massif. This specific structural setting is partly reflected in the course of torrents draining this part

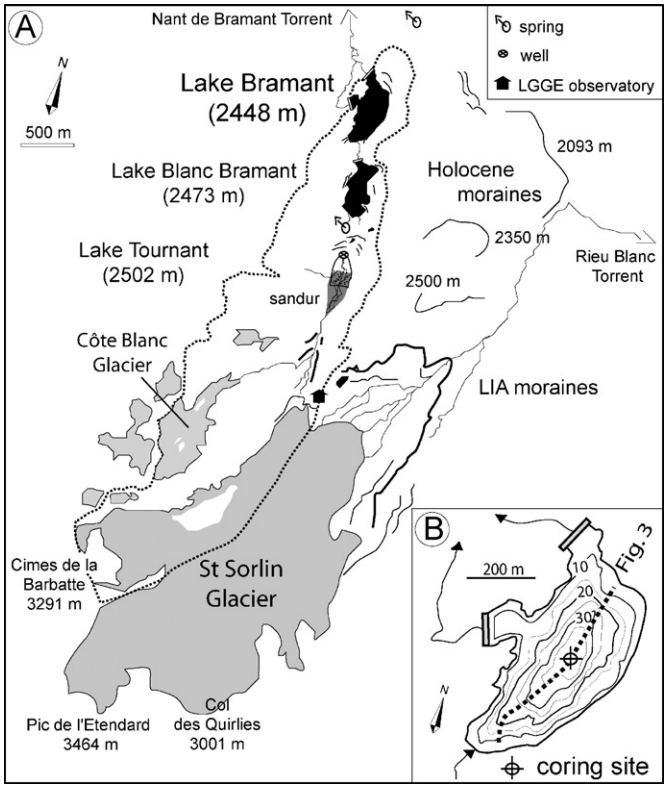

Fig. 2. Details of Lake Bramant catchment area. The catchment area (thick dotted line) consists of a chain of proglacial lakes draining the Côte Blanc glacier and a diffluence of the St. Sorlin glacier in the Bramant valley (A). All proglacial lakes in the Bramant valley were originally damned by frontal moraines, but since AD 1918, lakes Blanc Bramant and Bramant were enlarged by artificial dams to produce hydroelectricity. Up to five generations of moraines are recognized downstream from the St. Sorlin glacier: Holocene moraines (thin black lines), the Little Ice Age (LIA) moraines (thick black lines) and post LIA moraines (thin dotted lines). Lake Bramant bathymetry and the location of the coring site are based on seismic reflection profiling (B). The location of the seismic profile shown in Fig. 3 is indicated by a thick dotted line.

of the massif (Figs. 1b and 2a) and is associated with the occurrence of springs and wells at the contact of contrasted lithologies in the Bramant valley. Meltwaters from the diffluence of St. Sorlin glacier form a spring below recent frontal moraines and merge with Côte Blanc glacier meltwaters near fresh (but washed) lateral and frontal moraines formed in AD 1907 and during the LIA. These glacial meltwaters then feed a small sandur where fluvio-glacial streams are braided and today have almost completely filled proglacial Lake Tournant. The remnants of this uppermost proglacial lake are very shallow and the underground outlet feeds a spring at the base of grass-covered frontal moraines just upstream from Lake Blanc Bramant (Fig. 2a). Lake Blanc Bramant is deeper (17 m) and its outlet constitutes the main tributary of Lake Bramant, the lowermost of the three lakes. The two lower lakes were enlarged and deepened by dams built in AD 1918 to produce hydroelectricity until the 1980s.

In its natural state, Lake Bramant was dammed by frontal moraines and rock bars characterized by glacial

morphology. Today, it is located at 2448 m a.s.l, is 600 m long, 400 m wide and its maximum depth is ~39 m (Fig. 2b). Due to its specific geomorphologic relation with the St. Sorlin and Côte Blanc glaciers and due to its distal location in a chain of proglacial lakes, Lake Bramant only receives the fine-grained suspension load transported by glacier meltwaters. The drainage basin of Lake Bramant is small (ca. 5 km^2) and only locally covered by soils capped with alpine grassland. The catchment area is snow-covered more than 6 months per year. On average, the lake is largely frozen from mid-November to mid-June and tributary floods resulting from snowmelt events occur from mid-May to mid-July. Snow avalanches can reach the Eastern part of Lake Bramant and transport coarse particles from the catchment to the lake ice.

The Western Alps are also affected by large tectonic features such as basement thrusts and strike-slip faults (Thouvenot et al., 2003) and the study area has been historically subjected to several moderate magnitude earthquakes (Chapron et al., 1999; Arnaud et al., 2002; Nomade et al., 2005). Among them, the AD 1881 Allemond earthquake (intensity MSK VII) had an epicentre that was located less than 12 km away from Lake Bramant (Fig. 1).The AD 1822 Chautagne earthquake located at 90 km from Lake Bramant is the strongest of the study area (Fig. 1), with an estimated magnitude of 6–6.5 (Chapron et al., 1999).

In addition to these tectonic and climate changes, the massif has a long history of human settlement and land use since the Bronze Age (Bailly-Maître and Gonon, 2006) (Table 1). Evidence of a copper mining industry, developed between 2300 and 2650 m a.s.l. during the Early Bronze Age was indeed recently discovered in the massif, just SE of the catchment area of Lake Bramant (Bailly-Maître and Gonon, 2006; Bailly-Maître, oral communication). Furthermore, important silver and lead mining industry during the Middle Age (Table 1) is well-documented in the south western and western sides of the massif between 1800 and 2500 m a.s.l. (Bailly-Maitre and Bruno-Dupraz, 1994). According to the palynological studies of Chardon (1991) on the southern slopes of the massif near Alpe d'Huez (Fig. 2), alpine grasslands and trees appeared in our study area between 1800 and 2000 m a.s.l. with the first temperate phases of the Late Glacial period. Then, during the Atlantic pollen zone, a forest of birches and alders formed a transitional belt between coniferous subalpine forest and alpine grassland. This forest was clear cut during the Roman period (Table 1) and the present landscape of treeless grasslands became established above 1800 m a.s.l. On the other hand, no trace of mining activities during the Roman civilization has been discovered presently in the Massif.

3. Methods

3.1. Coring site

The sedimentary infill of Lake Bramant was imaged in summer 2003 with the ETH Zurich 3.5 kHz pinger system mounted on an inflatable boat. Conventional GPS navigation allowed the acquisition of a dense grid of high-resolution seismic profiles with a mean line spacing ranging between 50 and 100 m (Fig. 3). The system imaged an up to 20 ms two-way travel time (TWT) thick sedimentary succession and allowed the selection of a coring site in the depocenter of the basin. Following the seismic survey, two twin short gravity cores (BRA03-1, 80 cm long and BRA03-3, 70 cm long; 6 cm diameter) (Fig. 4) were taken in a water depth of 38.5 m from the inflatable boat with the ETH gravity corer. A month later, a 320 cm-long piston core (cored interval 190–510 cm below lake floor) (Fig. 4) with a diameter of 11 cm was then retrieved at the same site using a modified piston corer (Nesje, 1992) from the coring platform of Bergen University (Norway). The positions of the short gravity cores and the long piston core at site BRA03 were chosen in order to retrieve the best-possible undisturbed sediments above and below a large lens-shaped body with low-amplitude chaotic internal reflections covering most of the deep basin and being the thinnest at the coring site (Fig. 3). The absolute depth (below the lake floor) of the piston core was determined by core-to-seismic correlation: gamma density and P-wave velocity values of core BRA03 were measured at ETH at 0.5 cm intervals using a multi-sensor core logger (MSCL, Geotek Ltd.). The application of a mean P-wave velocity of 1500 m/s in the sediments allowed to correlate high-amplitude parallel reflections labelled R1 and R2 occurring at 440 and 480 cm below lake floor (Fig. 3), respectively, with abrupt changes in sediment density and lithology towards the base of the piston core (Fig. 4).

3.2. Multiproxy sediment core analyses

Cores were opened, described and photographed with a 400 d.p.i. resolution digital camera before *U-channels* were sampled in the middle of short core BRA03-1 and long core BRA03 in order to study geochemical and physical properties at very high resolution (Figs. 5–7) in undisturbed sediments (cf. Thomas et al., 2003; St-Onge et al., 2007). Total organic carbon (TOC) and traces of inorganic carbon (not shown) were measured at variable intervals in core BRA03 using a UIC 5001 coulometer at ETH.

CAT-Scan (computerized axial tomography) analyses were carried out at INRS-ETE (Québec City) with a pixel resolution of 1 mm.This non-destructive tool offers the ability to quantify and map X-ray attenuation coefficients of the sediment cores on longitudinal images (topograms). Data were processed with the Igor sofware according to St-Onge et al. (2007). The resulting images are displayed in greyscale with the darker grey representing lower X-ray attenuation and lower bulk density values (e.g., Crémer et al., 2002). Greyscale values can be extracted from the images and are expressed as CT numbers. A CT number is a complex unit related to the mineralogy, organic matter content, grain size and bulk density (Boespflug et al., 1995; St-Onge et al., 2007).

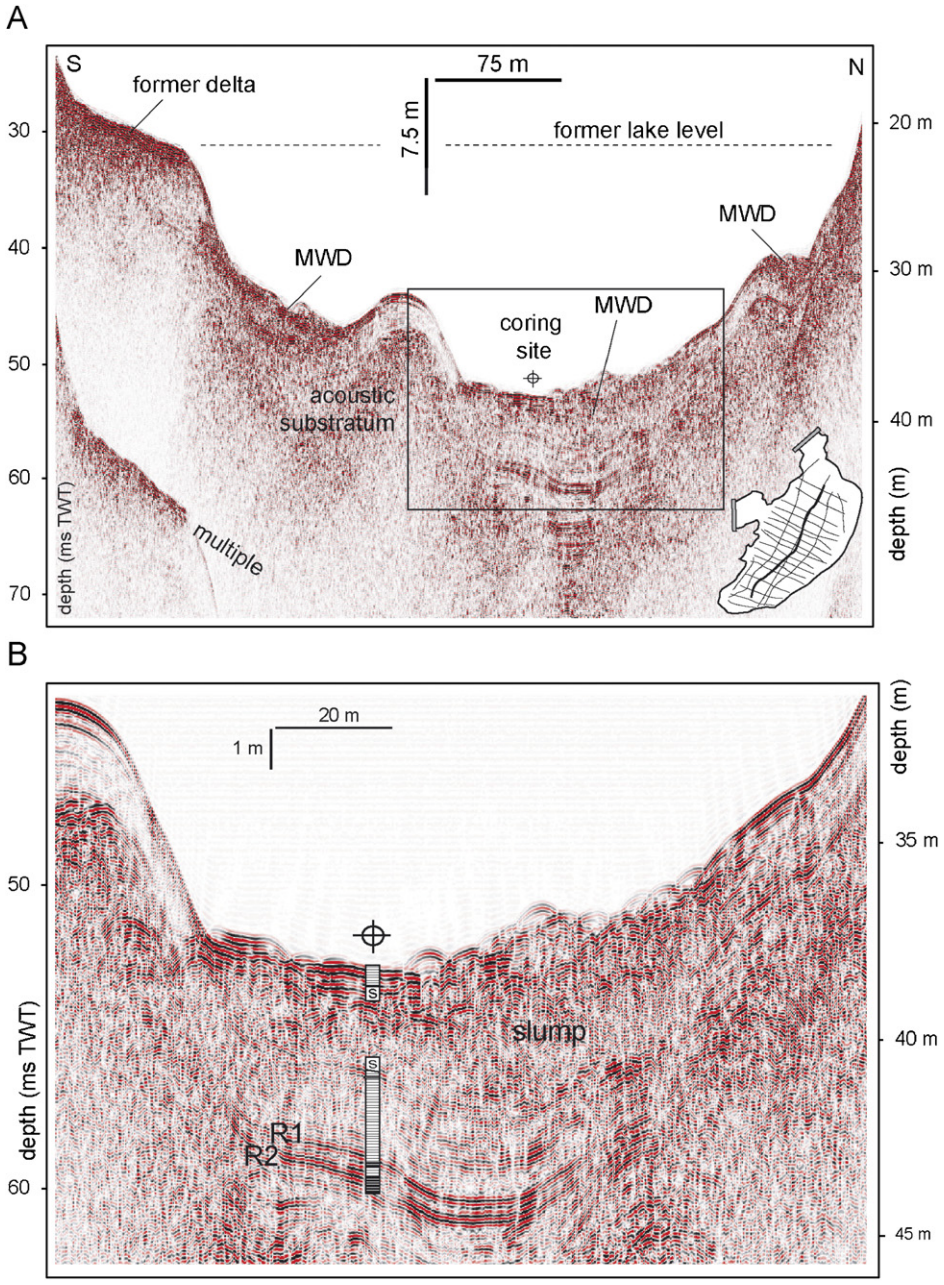

Fig. 3. Seismic profile (3.5 kHz) across Lake Bramant (A) and enlarged section illustrating the stratigraphy at the coring site (B). Undisturbed sediments were retrieved by short gravity cores and a long piston core above and below a large mass wasting deposit (MWD) as discussed in the text. This slump (S) and two high-amplitude reflectors (R1 and R2) are clearly visible in the deepest and thickest part of the basin.

Micro-fluorescence-X (XRF) analyses were made at the INRS-ETE with an ITRAX core scanner (Croudace et al., 2005; St-Onge et al., 2007) at a downcore resolution of 300 μm for BRA03-1 and 100 μm for BRA03. The ITRAX core scanner uses an intense non-destructive micro X-ray beam that irradiates the sample (during 10 s for BRA03-1 and 1 s for BRA03) to collect positive X-ray images and to detect the energy of fluorescent radiation in order to provide high-resolution relative concentration of elemental profiles (from Al to U). Radiographs obtained were transformed in negative X-ray images, in order to match the CAT-Scan images. The ITRAX images are 2 cm wide with a pixel size of 0.1 mm, while XRF analyses are measured from a 4 mm-wide and 0.1 mm-thick area. Elemental variations, given in peak area, are here standardized by rubidium, an element associated with fine detrital clays (Rothwell et al., 2006), in order to detect supplementary sources of geochemical elements different from the background concentration of detritic elements.

In short core BRA03-3, sediment grain size analyses were performed (not shown) at intervals ranging from 0.2 to 1 cm with a Malvern Mastersizer at Savoie University

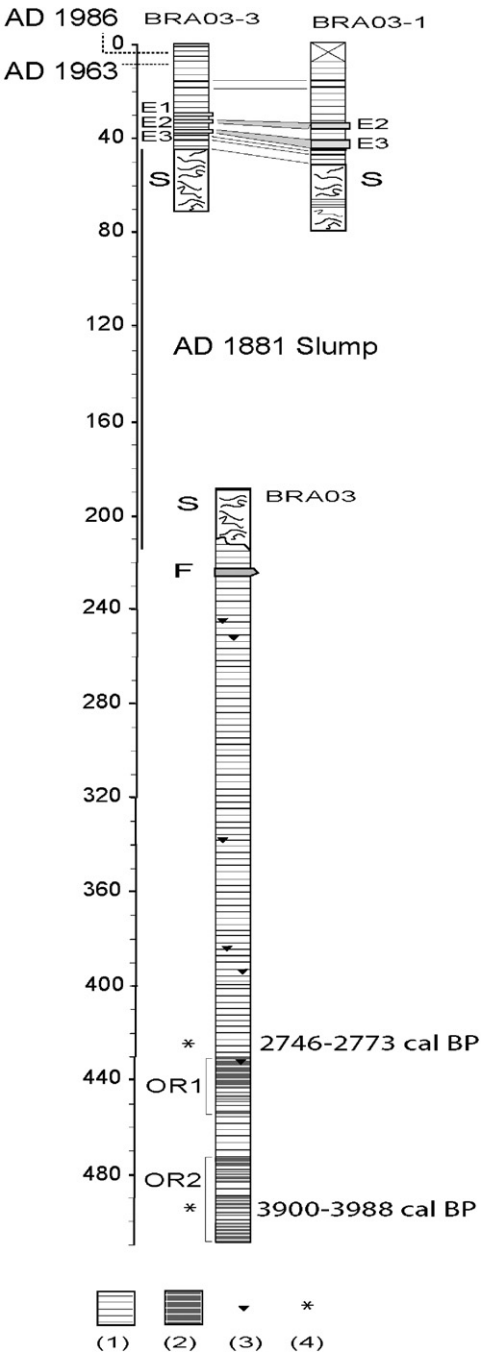

Fig. 4. General stratigraphy of the cores retrieved in Lake Bramant deep basin. Short gravity cores BRA03-1 and BRA03-3 above the slump (S) are correlated based on the occurrence of the sedimentary events (E1–E3) discussed in the text, while the depth of piston core BRA03 is based on the correlation of reflectors R1 and R2 with changes in the density of the sediments occurring in the organic layers OR1 and OR2, respectively. (1) finely laminated clastic sediments; (2) finely laminated organic-rich sediments; (3) drop stones; (4) AMS ^{14}C dates with a 1σ confidence limit.

(France), whereas in short core BRA03-1 and piston core BRA03, sediment grain size was determined at ISMER (Rimouski), with a sampling interval ranging from 0.5 to 2 cm depending on the studied facies. Prior to grain size analyses, the samples were added to a Calgon electrolytic solution (sodium hexametaphosphate) and rotated for about 3 h using an in-house rotator. The samples were then sieved (2 mm) and disaggregated in an ultrasonic bath for 90 s prior to their analysis. Disaggregated samples were then analysed with a Beckman-Coulter LS-13320 (0.04–2000 μm). The results of two and sometimes three runs were averaged. The average continuous disaggregated particle size distribution output was then processed using the Gradistat software for sediment parameters (Blott and Pye, 2001).

3.3. Chronology

Two terrestrial plant debris, found at 423 and 493 cm below lake floor in core BRA03, were extracted and dated by accelerator mass spectrometry (AMS) ^{14}C at the Poznan Radiocarbon Laboratory in Poland (Table 2). They were reported using Libby's half-life and corrected for natural fractionation ($\delta^{13}C = -25‰$). The ^{14}C ages were calibrated in calendar years using the online calibration software CALIB 5.0.2 (Stuiver et al., 2005) using the Reimer et al. (2004) dataset and are shown using a 1δ or 2δ confidence interval (Table 2).

The chronology of short core BRA03-3 is provided by radionuclide dating (^{137}Cs and ^{241}Am). The sampling interval was every 0.5 cm for the first 10 cm, and every 1 cm from 10 to 37 cm (i.e., 48 sediment samples in total). Samples were dried at 60 °C for 3 days and homogenized with a pestle and a mortar before conditioning and analysis in gamma spectrometry. The samples were then sealed and left for 3 weeks to allow equilibrium between ^{226}Ra and supported ^{210}Pb. The samples were then analyzed in a low background germanium well detector (Canberra Company). All the radiometric measurements were performed in a very low-level background laboratory at the LGGE, France. Details of the methods are given in Pinglot and Pourchet (1995).

Short core BRA03-1 is correlated to BRA03-3 based on the identification of several sedimentary events evidenced in both cores by digital photographs and grain size analyses. The chronology is ripened by the establishment of annual sedimentation record (i.e glacial varves). Varve counting in short cores and piston cores based on the core photographs, the CT number and/or Fe peak counting are further confirmed by the recognition of robust chronostratigraphic markers, such as historical earthquakes (see Section 6.1.1), or known periods of mining activities (see Section 6.2.2.).

4. Results

4.1. Basin fill characteristics

Seismic profiling shows limited deposition of sediments above the isobath 20 m, but a delta front occurs at 22 m water depth in the southern part of the basin, as well as a sediment depocentre in the basin below ca. 30 m water

Table 2
Radiocarbon ages

Depth (cm b.l.f.)	^{14}C age (yr BP)	Calibrated ages (1σ) (cal BP)	Calibrated ages (2σ) (cal BP)	Material	Laboratory ref.
423	2635±35	2746–2773	2713–2789	Terrestrial plant debris	POZ-13991
493	3650±35	3900–3988	3868–4020	Terrestrial plant debris	POZ-13993

The two dates were calibrated using the online calibration software CALIB 5.0.2 (Stuiver et al., 2005) using the Reimer et al. (2004) dataset. The calibrated ages used in the age model (Fig. 14) were calculated as the mid-point of the 1δ confidence interval.

depth (Figs. 2B and 3). In this deep part of the basin, the infill is characterized (i) by the deposition of three recent coeval lens-shaped bodies, made of chaotic to transparent acoustic facies, and (ii) by the occurrence of two high-amplitude and continuous reflectors, labelled R1 and R2. R1 and R2 are only present in the deepest part of the main basin and are clearly contrasting with the dominating acoustic facies, consisting of low-amplitude and poorly continuous reflections (Fig. 3).

Sediment cores retrieved in the deepest part of the basin consist of light-grey to dark coloured finely laminated sandy silts that are containing few angular drop stones throughout the cores as shown in Fig. 4. Striking sedimentary deposits labelled E1, E2, E3, S and F (see Guyard et al., in press) are intercalated within the uppermost 2.4 m of the basin fill (Figs. 4–6).

4.2. Dominating sedimentary facies

At the base of the piston core BRA03, darker-coloured finely laminated intervals are recorded between 429 and 455 cm (OR1) and between 473 and 508 cm (OR2) below lake floor (Figs. 4, 5 and 7) and correspond to the seismic reflectors R1 and R2, respectively (Fig. 3). They are characterized by coarser sediments (only 17% of fine silts), an increase in organic carbon (up to 3%, Fig. 7) and a fall in gamma density (Fig. 5). The fall in bulk density is also reflected by the lower CT number values and the darker grey scale observed on ITRAX images (Fig. 7). The higher organic matter content in intervals OR1 and OR2 is also suggested by the ratio of incoherent over coherent scattering (inc/coh) measured during core irradiation by the ITRAX core scanner (Fig. 7). The number of incoherent scattering between electrons is—in theory—higher for elements with a low atomic mass. The inc/coh ratio is therefore linked to the mean atomic number and could be partly related to carbon content. This relationship is confirmed by the correlation between TOC measurements and inc/coh ratio, shown on Fig. 7. These organic-rich intervals are furthermore strikingly rich in sulphur and have higher Fe/Rb, Ca/Rb and Mn/Rb contents (Fig. 7). Throughout the core Fe, Ca and Mn are well correlated with Fe/Rb ($r = 0.93$) (Fig. 8), Ca/Rb ($r = 0.98$), and Mn/Rb ($r = 0.73$), respectively. As shown in Fig. 8, elements that are usually interpreted to be of detrital origin such as Si, K and Rb are well-correlated together ($r = 0.94$ between K and Rb). It is also worth noting that OR1 and OR2 are associated with a fall in fine detrital elements, represented here by Rb contents.

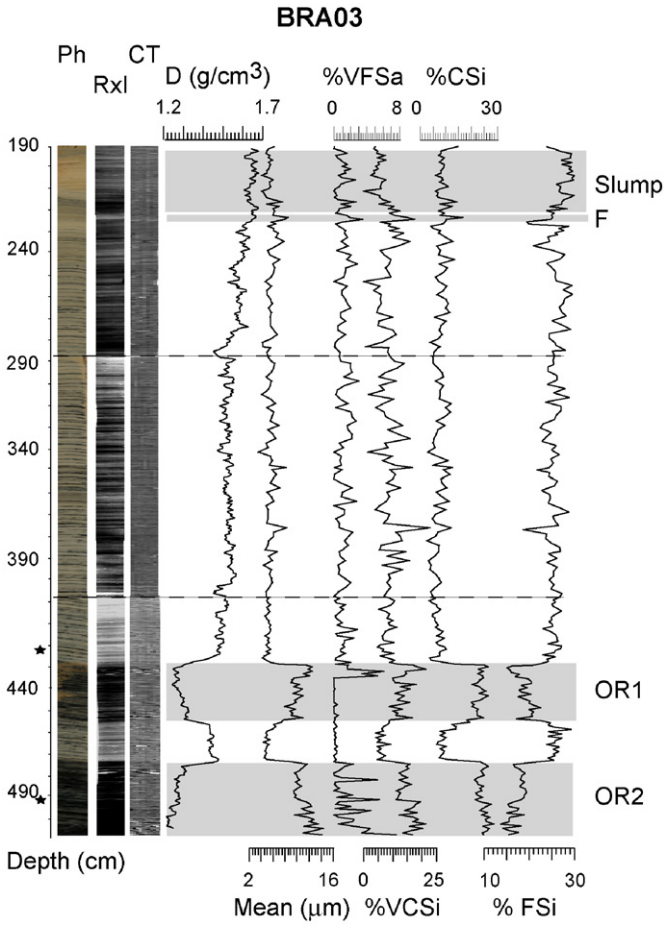

Fig. 5. Grain size parameters and gamma density for core BRA03. Ph: numerical photography (core breaks are illustrated by dotted lines); RxI: X-ray image obtained on u-channel samples by ITRAX; CT: topogram obtained on u-channel samples by CAT-Scan; D: gamma density (g/cm^3); Mean: mean grain size (µm); VFSa, VCSi, CSi and FSi: very fine sand (63–125 µm), very coarse silt (31–63 µm), coarse silt (16–31 µm) and fine silt (4–8 m) percent, respectively. Location of plant debris used for AMS ^{14}C dating are illustrated by stars.

Between both organic intervals (455–473 cm) and after OR1 (from 429 to 217 cm), an abrupt onset of more clastic sedimentation occurs (Figs. 4, 5 and 7). These finely laminated sediments are characterized by a lighter colour, an abrupt increase of fine silt percent (up to 26% of the

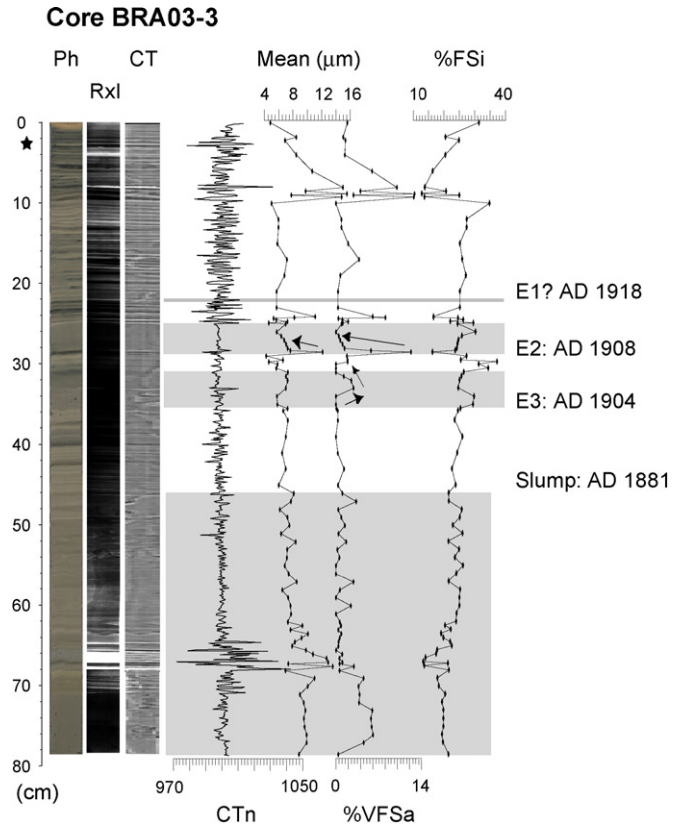

Fig. 6. Multiproxy analysis of BRA03-1 gravity core. Ph: digital photography; RxI: X-ray image obtained on u-channel by ITRAX core scanner analysis; CT: topogram obtained on u-channel by CAT-Scan analysis; CTn: CT number; Mean: mean grain size (µm); %VFSa: % of very fine sand (from 63 to 125 µm); %FSi: % of fine silt (from 4 to 8 µm). The age of the sedimentary events was determined by counting the CT number peaks from the top of the slump to the top of the core and confirmed by "Fe peak counting". AD 1963 level estimated location is obtained by varve counting (see text for details) and illustrated by a star.

sediment; Fig. 5) and an abrupt rise in bulk density. These sediments are also characterized by an increase in the concentration of detrital elements (Si, K, Rb), but by a decrease in the concentration of organic carbon, Fe, Ca and Mn content. Moreover, the sorting vs. skewness diagram highlights two different grain size distribution patterns (Fig. 9) between these clastic and the more organic facies OR1 and OR2 where the clastic sediments are poorly sorted and symmetrical, whereas organic-rich sediments are poorly sorted and fine skewed.

4.3. Finely laminated facies

Throughout the cores, the sediments are characterized by a fine lamination made of light and dark-coloured laminae as shown in Figs. 5–7 and 10. Lighter-coloured layers are rich in detrital elements, such as Rb, Si, or K (not shown), have a higher bulk density and a finer mean grain size. On the other hand, darker layers contain less detrital elements but are rich in Fe, Ca or Mn. They are also coarser and characterized by higher values of inc/coh, suggesting a higher content of organic content than in the light-coloured laminae.

4.4. Sedimentary events

Between 227 and 224 cm below lake floor, event F is characterized by an erosional basal contact, a coarse grained base rich in very coarse silts and a fining upward sequence as shown by mean grain size, CT numbers and the lighter X-ray images (Figs. 5, 7 and 11). Mud clasts are also observed on the Rx images from 226 to 224 cm (Guyard et al., in press).

The chaotic acoustic facies identified by seismic analysis (Fig. 3) was only retrieved at the base of the short gravity cores and the top of the piston core, as shown in Figs. 3 and 4, confirming the seismic interpretation that the non-cored interval (70–190 cm below lake floor) only consists of disturbed sediments (i.e., a mass wasting deposit (MWD)). The base of this disturbed interval is observed at 217 cm in core BRA03, just above deformed laminae deposited during a normal sedimentation period (Figs. 5, 7 and 11). The upper limit of disturbed sediments is observed at 44.5 cm depth in core BRA03-3 and at 46 cm depth in BRA03-1 (Figs. 4 and 6). Sediments have a lighter colour with regards to the rest of the core and are remoulded, folded, laminated and highly deformed in specific intervals. Sediments are also locally composed of cross laminations, erosive contacts and blocks of sediments with the preserved original stratification as seen on topograms (Figs. 5–7, and 11). Locally, relatively well-stratified sediments documented by CAT-scan images within the lower part of these remoulded deposits are enriched in lead between 216 and 206 cm (Fig. 11).

The deposit labelled E1 is a 0.8 cm-thick graded layer observed at 27–28 cm in BRA03-3, but is unrecognized in core BRA03-1 (Fig. 4). Deposits E2 (observed at 32–33.5 cm in BRA03-3 and at 25–28 cm in BRA03-1) and E3 (observed at 35–37 cm in BRA03-3 and at 31–35 cm in BRA03-1), are coarser graded layers (Fig. 6). In core BRA03-1, E3 is a 4-cm thick graded bed with a basal sequence developing an inverse grading (coarsening upward) and an upper sequence with normal grading (fining upward) (Fig. 6). In core BRA03-1, the distribution of very fine sand and of mean grain size in the 3-cm thick deposit E2 depicts a normally graded sequence starting with a sharp basal contact and a coarse base. This fining upward sequence has no visible structures on CAT-scan and X-ray images (Fig. 6).

4.5. Metallic contaminations

ITRAX data are highlighting a major peak in lead content (peak areas are up to 12 times higher than the background), a clear peak in copper content (Fig. 7) and in zinc content (not shown) between 340 and 357 cm. This heavy metal contamination culminates between 350 and

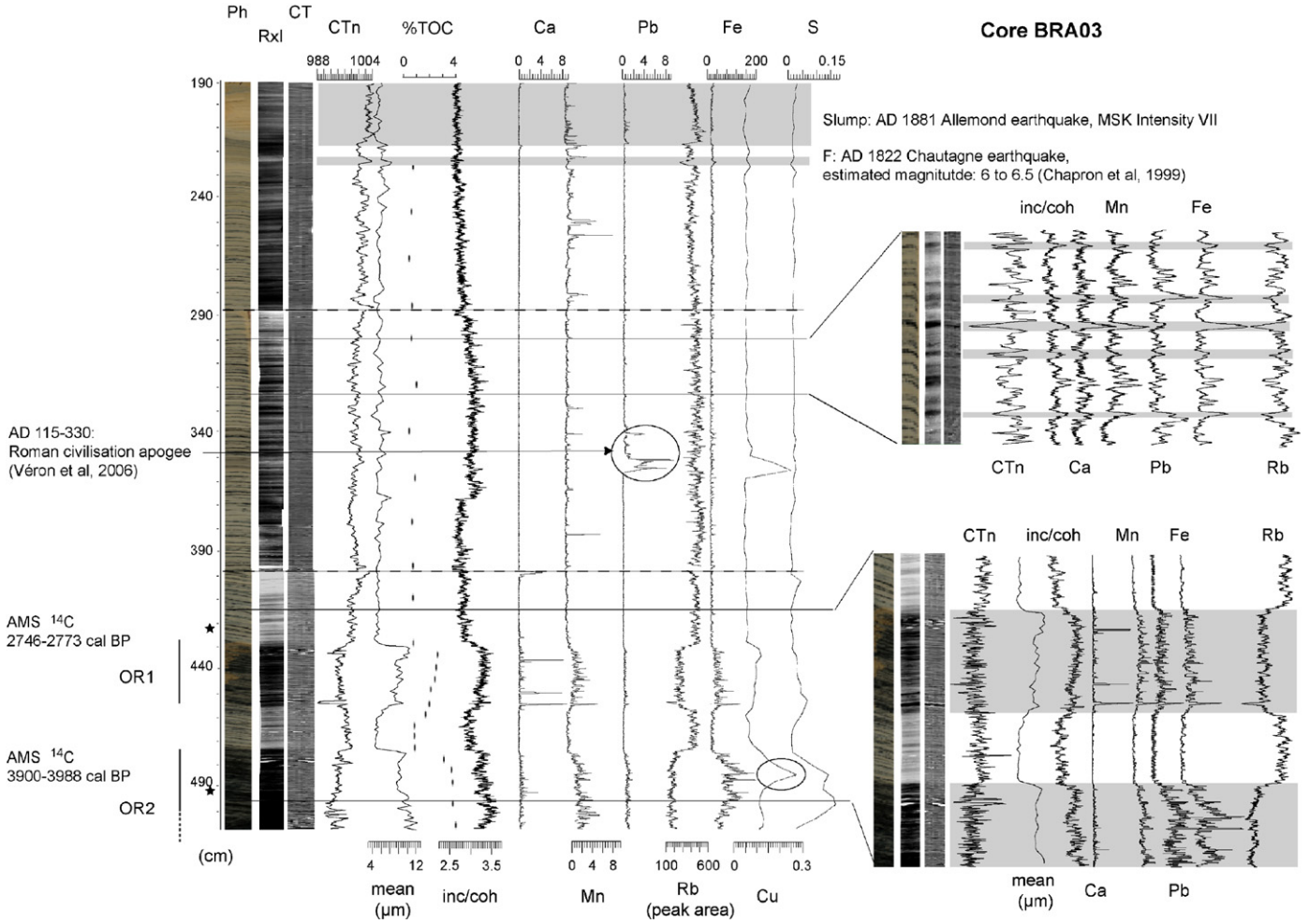

Fig. 7. Multi-proxy analysis for piston core BRA03. Ph: numerical photography (core breaks are illustrated by thin dotted lines); RxI: X-ray image obtained on u-channel samples by ITRAX; CT: topogram obtained on u-channel samples by CAT-Scan; CTn: CT number. Illustrated is an 11-point smooth except for the zoom (right part of the figure) on laminations and organic levels (see text for details). TOC: % total organic carbon. Ca, Mn, Pb, K, Fe, S and Cu are normalized by Rb.

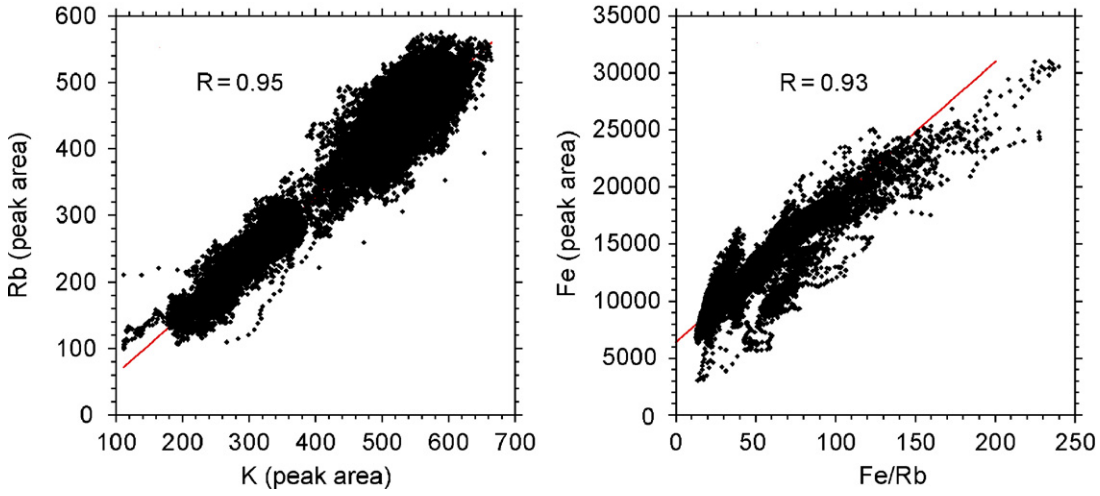

Fig. 8. Rb plotted vs. K and Fe/Rb plotted vs. Fe.

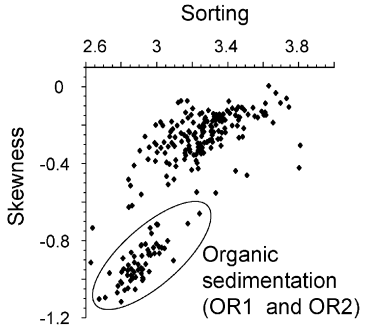

Fig. 9. Skewness vs. sorting diagram. Samples from the organic-rich layers OR1 and OR2 are circled.

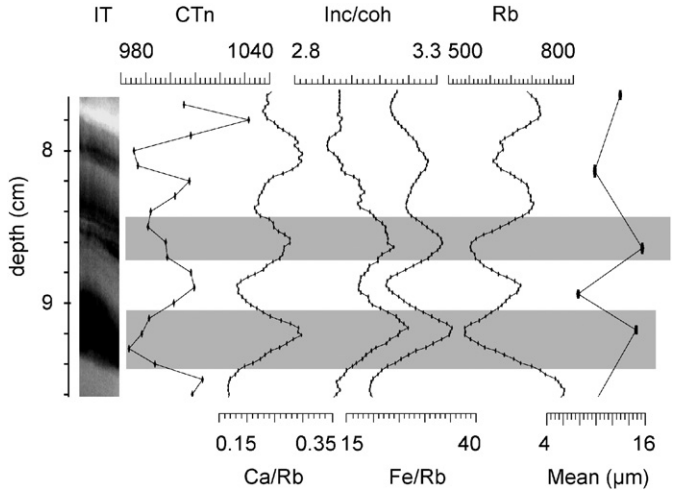

Fig. 10. Main characteristics of dark laminations between 8 and 9.5 cm in core BRA03-1. Dark laminations have a lower CT number (a bulk density proxy) and Rb content, but higher Fe and Ca contents, a larger mean grain size and a higher inc/coh ratio (a proxy of organic matter content). Fe/Rb, Ca/Rb, Inc/coh and Rb: illustrated are an 11-point-smooth.

356 cm. In addition, another striking peak in copper is clearly detected on ITRAX data between 483 and 489 cm (Fig. 7).

4.6. Radiocarbon and artificial radionuclides

In piston core BRA03, the ^{14}C ages obtained at 423 cm and at 493 cm correspond to 2746–2773 cal BP and to 3900–3988 cal BP, respectively (Table 2). These ages, covering the Bronze Age period, have provided the basis for the age–depth model of the piston core (see Section 5.3).

In short core BRA03-3, the ^{137}Cs and ^{241}Am artificial radionuclide concentrations are highlighting a sharp peak between 8 and 9 cm (Fig. 12). Above this sharp peak in ^{137}Cs reaching 700 mBq/g, a second and smaller peak with specific activities close to 400 mBq/g is occurring between 2.5 and 3 cm.

5. Annual laminations and chronology

5.1. Annually laminated sediments

Following the studies of Appleby et al. (1991), Arnaud et al. (2002) and Nomade et al. (2005), the sharp peak in ^{137}Cs and ^{241}Am concentrations measured in core BRA03-3 is related to the culmination in AD 1963 of atmospheric nuclear tests in the northern hemisphere, and the second smaller peak in ^{137}Cs, to the Chernobyl (Ukraine) nuclear reactor accident in 1986. This interpretation is supported by the counting of 26 couplets of dark and light-coloured laminae on digital photographs between 2.5 and 8.5 cm, suggesting the formation of annual lamination in Lake Bramant during the 1963–1986 time span (23 years).

The formation of an annual lamination resulting from the deposition every year of a dark lamina rich in Fe and a light lamina rich in Rb in Lake Bramant sediments is confirmed at the base of piston core BRA 03 by counting ~1220 Fe fluctuations between the two available radiocarbon ages at 493 cm (3944 ± 44 cal BP) and 423 cm (2760 ± 13 cal BP), corresponding to a time period of 1175 ± 58 years.

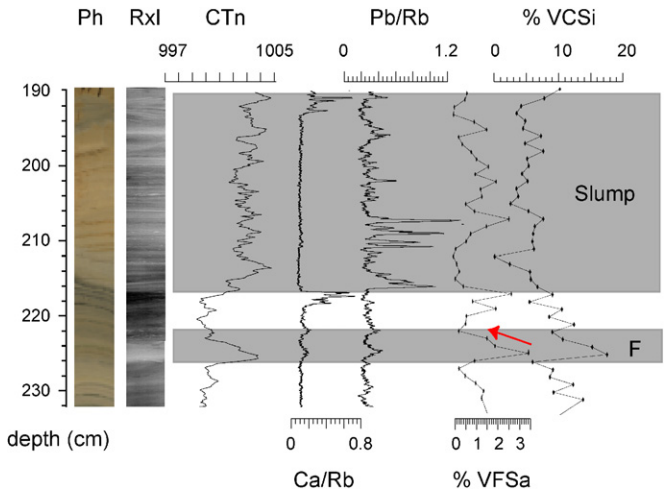

Fig. 11. Multiproxy details of the AD 1881 slump base and of the AD 1822 earthquake-triggered turbidite deposit (labelled F). Lead peaks in the slump deposit probably correspond to a remobilization of contaminated sediments by the mining exploitation during the Roman civilization.

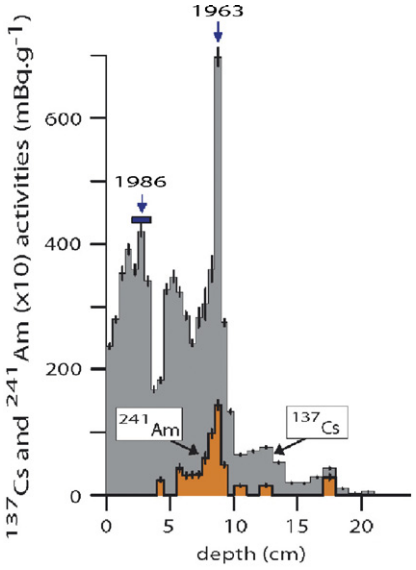

Fig. 12. Radionuclide massic activities in core BRA03-3. Peaks in AD 1963 and 1986 are highlighted.

5.2. Origin of the annual laminations

As shown above by laminae counting and radionuclides, the dark and light-coloured couplets are varves. High correlation coefficients between Fe and Fe/Rb (see Fig. 8), between Ca and Ca/Rb and between Mn and Mn/Rb suggest that Fe, Ca and Mn are mainly formed in situ, whereas K and Rb are proxy of fine detrital sediment fluctuations. Higher values of inc/coh in darker laminae (Figs. 7 and 10) suggest a higher organic matter content in these layers. Consequently, the dark laminae rich in neoformed elements are interpreted as the product of calm background sedimentation, while the lighter layers, rich in detrital elements, are interpreted as resulting from the summer snowmelt. Smaller mean grain size in the lighter layer (Fig. 10) essentially reflects the deposition of the fine-grained sediment suspension load, as lakes Tournant and Blanc-Bramant (Fig. 2) are acting as sediment traps for the coarser sediments transported by glacier meltwaters during the summer snowmelt.

5.3. Chronology

5.3.1. Age–depth model in short cores

In short core BRA03-3, varve counting using digital photographs below the AD 1963 peak allows to date the deposit E1 at AD 1917. E1 is interpreted as a turbidite triggered by the impact of the construction of hydroelectric dams (Fig. 2) that flooded the natural lake in AD 1918. Following the same method, the deposits E3 and E2 are dated to ca AD 1905 and 1910, respectively, whereas the top of the MWD is dated to ca AD 1886. As discussed in Section 6.1.2, deposits E3 and E2 are interpreted as large flood deposits, whereas the MWD is correlated to the impact of the nearby AD 1881 Allemond earthquake (Figs. 1 and 2). Historic ages (AD 1881 and AD 1918) were thus used to construct the age model for short core BRA03-1.

In core BRA03-1, varve counting using high-resolution CAT-Scan and XRF analyses (Figs. 6 and 13) from the top of the AD 1881 MWD allows to date deposits E3 and E2 at AD 1904 and AD 1908, respectively. Ascending to the top of the core, the year AD 1918 is placed at 22 cm depth and sediments dated to AD 1963 are recorded at 2.9 cm depth, confirming that the mud line (i.e. the uppermost 8 cm of sediments) were not retrieved in this core, as shown in Fig. 4.

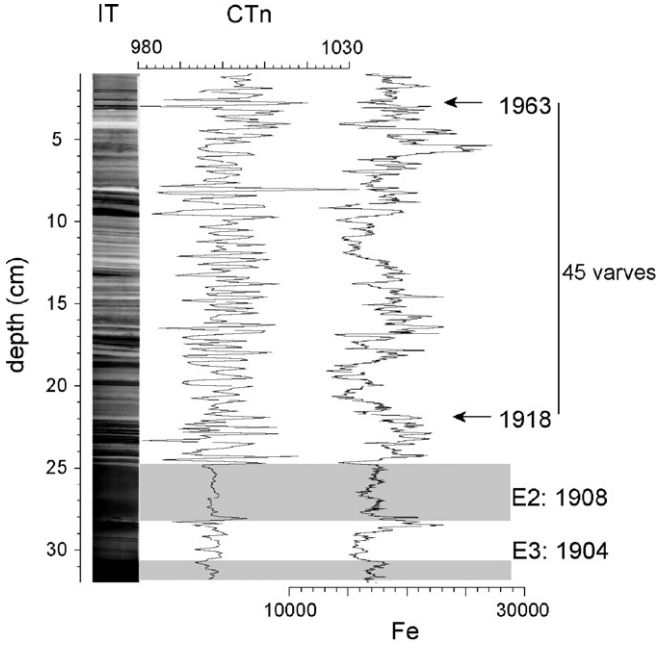

Fig. 13. Details of the age–depth model in the upper part of core BRA03-1. The varves were counted by "CT number peak counting". IT: Rx obtained by ITRAX core scanner analysis; CTn: CT number.

Mean sedimentation rates are slightly falling from 4.6 to 4.2 mm/yr after the construction of the hydro-electric dam in AD 1918. The impact of the dam construction since AD 1918 on lacustrine sedimentation is notably highlighted by the onset of thinner laminations, suggesting that the dam in Lake Blanc Bramant acts as a retention basin (cf. Vörösmarty et al., 2003; Syvitski et al, 2005).

5.3.2. *Age–depth model in piston core*

In piston core BRA03, Fe peak counting below 493 cm gives an age around 4160 ± cal BP to the base of the core (Fig. 14). Ascending from 2760 cal BP to the top of the core, the strong contamination in lead and copper identified between 340 and 357 cm (Figs. 7 and 14) is dated to AD 115 to AD 330 and culminates between AD 130 and AD 210. As discussed in Section 6.2.2, this peak is interpreted as resulting from mining activities during the Roman civilization (Table 1), whereas the copper anomaly identified between 483 and 489 cm and corresponding to 3770–3870 cal BP is related to a local mining industry occuring during the Early Bronze Age (Bailly-Maitre and Gonon, in press). Following the same dating procedure, the base of event F is dated to ca AD 1800 and could thus be correlated with the strongest historical earthquake of the study area (Fig. 1): the AD 1822 Chautagne earthquake (estimated magnitude: 6–6.5). Similarly, the number of Fe peaks between the top of deposit F and the base of the AD 1881 MWD, suggests that this uppermost earthquake-triggered deposit overlies sediments dated to about AD 1850. As summarized in Fig. 14, mean sedimentation rates in Lake Bramant slightly increased at the beginning of the Iron Age (from 0.6 to 0.71 mm/yr) and slightly rose to ca. 0.76 mm/yr after the Roman period. These sedimentation rate fluctuations are likely connected to environmental changes resulting from both climate and human impact in the drainage basin.

As discussed in the following sections, the varved-based age–depth models are further supported by the identification of known periods of local or regional mining activities during the Early Bronze Age and the Roman civilization and by the identification of historical events, resulting from local or regional seismicity or from climate change.

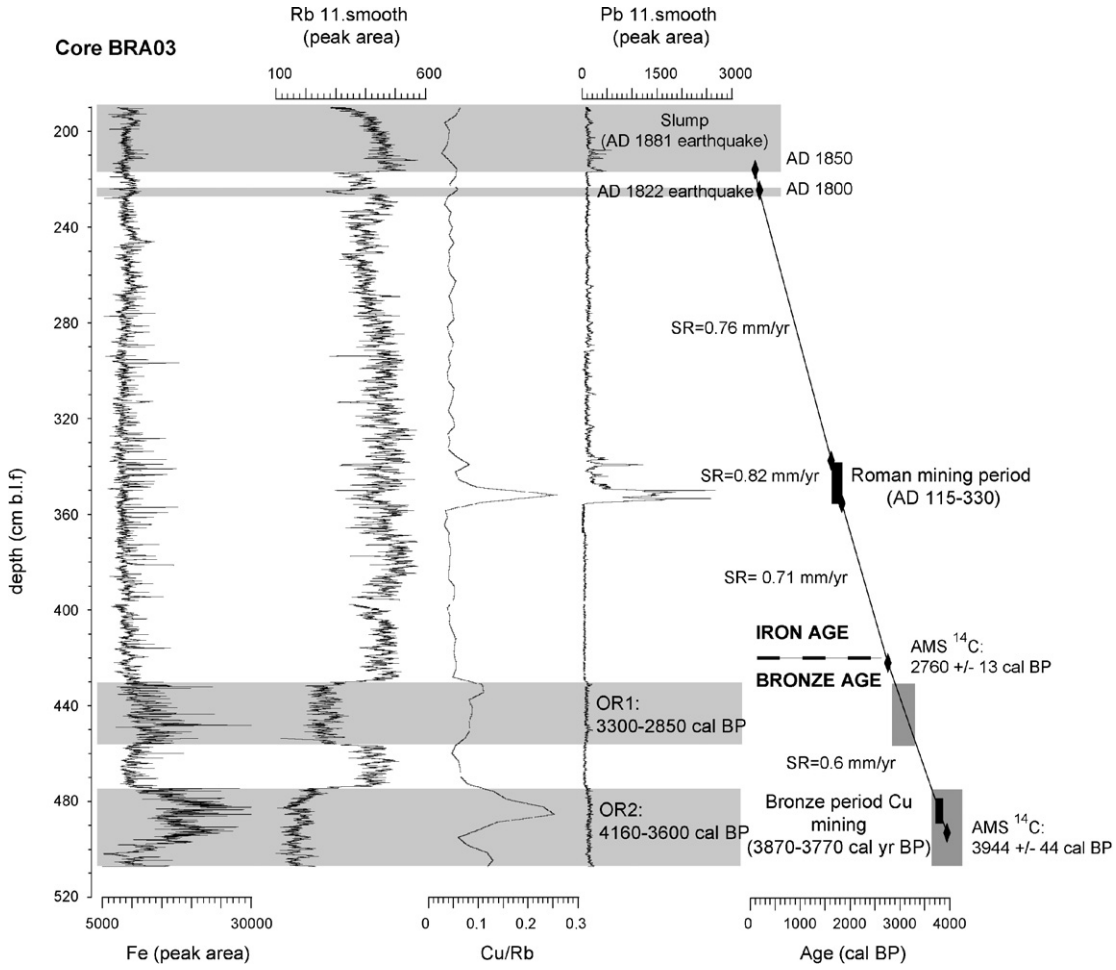

Fig. 14. Age–depth model below the slump. The age model is based on two radiocarbon dates and varve counting as discussed in the text. Varve counting is supported by the identification of metallic contaminations in the sediments during the Bronze Age and the Roman periods. Also illustrated are the metallic contamination during these periods, as well as the fine detrital grain (Rb) and neoformed elements (Fe/Rb) profiles.

6. Discussion

6.1. Sedimentary records of natural hazards

6.1.1. Historical earthquakes

Paleoseismologic studies using lake sediments are frequently based on the detailed characterization of contemporaneous sedimentary events related to subaqueous slope failures and on the establishment of a precise chronology. Since single mass wasting deposits such as slumps or turbidites could also be produced by other processes (lake level change or slope overloading, for instance), the best argument to asses a seismic triggering is to correlate such sedimentary event with a well-documented historical earthquake (Doig, 1986; Siegenthaler et al., 1987; Chapron et al., 1999; Arnaud et al., 2002; Schnellmann et al., 2002; Monecke et al., 2004; Nomade et al., 2005).

In Lake Bramant, we have shown that a major MWD affecting most of the deep basin (Fig. 3) can be correlated to the AD 1881 Allemond earthquake (Fig. 1). This interpretation is in agreement with the occurrence of several MWD on seismic profiles just below the lake floor (Fig. 3), suggesting that unstable sediments in the lake were mobilized by earthquake ground accelerations in AD 1881 in various simultaneous mass flows, a criteria used previously to single out earthquake shaking as trigger mechanism (Schnellmann et al., 2002; Strasser et al., 2006). This event had a MSK intensity of VII near Allemond and its epicentre was located less than 12 km from Lake Bramant (cf. Nomade et al., 2005 and references therein). This event was both strong and close enough to trigger mass wasting events in Lake Bramant. The deformed background sediments likely result from the rapid deposition of an important quantity of sediments (1.10 m at the coring site). This earthquake-induced mass movement is an example of a rotational sediment slide (Locat and Lee, 2002), corresponding to a slump following the classification of Mulder and Cochonat (1996). Lead concentrations in Lake Bramant sediments incorporated in the base of the slump could result from remoulded sediments of Roman mining period.

The occurrence of a sharp contact at the base of layer F, the normal grading and the presence of mud clasts in the fine layer F is suggesting the formation of an incomplete Bouma turbidite (e.g., Bouma, 1962; Mulder et al., 2001), where only facies Ta-Tb were recorded. This turbidite, dated to AD 1800 was probably triggered by the AD 1822 Chautagne earthquake, the strongest of the region with an estimated magnitude of 6–6.5 (Chapron et al, 1999).

It is, however, much more delicate to correlate the 5-cm thick graded layer labelled event E3 dated between AD 1904–1905 with the AD 1905 Emosson earthquake (MSK intensity VII–VIII; Fig. 1). The epicentre of this event was located near the French/Swiss border and it was recorded in the nearby Lake Anterne (Arnaud et al., 2002), but was probably too far away (more than 160 km) from Lake Bramant to trigger slope instabilities that resulted in the basin centre in the deposition of a turbidite. As discussed below, the origin of this graded bed may therefore be related to a large flood event, as sedimentary event E2.

6.1.2. Exceptional flood events

Sedimentary event E3 (Fig. 6) is bearing the typical grain size distribution of large flood events deposited by hyperpycnal flows in marine or lacustrine environments (cf. Syvitski and Schafer, 1996; Mulder et al., 1998; Schneider et al., 2004; St-Onge et al., 2004; Chapron et al., 2006; Guyard et al., in press; St-Onge and Lajeunesse, in press): a basal sequence developing an inverse grading (coarsening upward) during the rising limb of the flood (waxing flow) and an upper sequence with normal grading (fining upward) during the falling limb of the flood event (waning flow). Sedimentary event E2 (Fig. 6) is interpreted as a large flood-triggered turbidite either related to the development of a large homopycnal flow across the lake (cf. Brodzikowski and Van Loon, 1991), or related to the formation of a hyperpycnal flow where only the upper sequence was preserved because of strong erosion during the rising limb of the flood (cf. Mulder et al., 2001, 2003). In both cases, this flood deposit triggered between AD 1908 and 1910 was probably an erosive event. The formation of such exceptional flood deposits in Lake Bramant may result from exceptional snowmelt events, heavy rainfalls during the summer or, more probably, from the catastrophic drainage (i.e. outburst) of a temporary ice-contact lake or even a subglacial lake. Temporary ice marginal lakes are frequently observed at the margin of the St. Sorlin glacier near its diffluence into the Bramant valley (M. Vallon, pers. comm.) and subglacial lakes may have also formed in the past below St. Sorlin or Côte Blanc glaciers. According to the age–depth model and to first field observations in AD 1907 (Fuselin et al., 1909), the exceptional flood events E2 and E3 occurred when the St. Sorlin glacier was already retreating from its last advance following the end of the LIA. It seems therefore likely that exceptional flood deposits in Lake Bramant are synchronous with periods of important glacier retreat.

6.2. High-altitude environmental changes

6.2.1. Glacier and lake level fluctuations

Variations in the amount of organic or clastic constituents accumulated in proglacial lake sediments are often used as proxies for glacier activity in the drainage basin (cf. Dahl et al., 2003 and reference therein). Variations of the Rb content are related to fluctuations in the amount of detrital clays (cf. Rothwell et al., 2006). Rb content in Lake Bramant reflects the finer sediment supply resulting from glacial erosion (the "glacial flour"). Both organic intervals OR1 and OR2 are clearly contrasting with the recent proglacial sediments and the occurrence of reflectors R1 and R2 only in the deepest part of the basin suggests the

development of very different environmental conditions. Such an organic sedimentation, associated with a fall in detrital elements and with a limited percent of fine silts, suggests reduced glacier activity and glacial erosion in the catchment area.

OR2 is deposited during the Early Bronze Age (Table 1) between 4160 and 3600 cal BP. A very good correlation between S and S/Rb (not displayed) in both organic facies ($r = 0.81$) likely reflects the development of anoxic conditions. In these layers, higher neoformed elements contents like Fe, Ca, or Mn also suggest very different depositional environments in a much smaller and shallower lake than in the rest of the core. A more detailed study is nevertheless needed to define the nature of iron-rich precipitated elements. Taken together, these characteristics are interpreted as resulting from a phase of low lake level and reduced glacier activity in this part of the Alps between 4160 and 3600 cal BP. This is in agreement with the occurrence of lower glacier activity in the Swiss Alps (Leeman and Niessen, 1994) and a phase of low-lake level in west-central Europe (Magny, 2004; Holzhauzer et al., 2005).

Above OR2, between 3600 and 3300 cal BP, the abrupt return to more clastic sedimentation in Lake Bramant is interpreted as an increase in glacier activity and glacial erosion. During this short period, the diffluence of the St. Sorlin glacier into the Bramant valley was probably important enough to provide glacial meltwaters rich in fine-grained particles to Lake Bramant. This is in agreement with a wetter and colder period during the mid-Bronze Age documented by a high lake-level period between 3500 and 3100 cal BP in west-central Europe (Magny, 2004; Holzhauzer et al., 2005) and the onset of a neoglaciation marked by glacial varve formation since 3300 cal BP in the proglacial lake Silvaplanna, Swiss Alps (Leeman and Niessen, 1994). It is likely that the level of Lake Bramant was also higher and oxygenated during this episode since no sulphur were found in the sediments.

The upper organic interval (OR1), with the same characteristics than OR2, was formed between 3300 and 2850 cal BP. During this Late Bronze Age period, Lake Bramant was thus probably at a lower level because the St. Sorlin glacier was likely too reduced to develop a clear diffluence into the Bramant valley. This phase of reduced glacier activity is not clearly recorded in Lake Silvaplana (Leeman and Niessen, 1994), but suggested in the study of Holzhauzer et al. (2005) by glacier and lake-level fluctuations.

The coarser grain size observed in the organic-rich intervals OR1 and OR2 probably reflects changes during the Bronze Age in the size of the lake and especially in the ratio between the surface of the lake and the surface of the drainage basin. This ratio is both controlling the influence of particles streaming versus deltaic sedimentation and the residence time of the lake waters (Meybeck, 1995). Different grain size sorting and skewness values in organic and clastic sediments (Fig. 9) are also suggesting sedimentation under rather calm hydrodynamic conditions during Bronze Age periods with low-lake levels, but more turbulent ones during clastic dominated sedimentation.

At 2850 cal BP, the abrupt return to clastic sedimentation (i.e. high density, low mean grain size due to the increase of the fine silts, low organic matter content, absence of sulphur in the sediments and an increase in detrital elements) is interpreted as increasing glacier activity and glacial meltwaters supply in the Bramant valley, favouring high-lake levels in the chain of proglacial lakes. The onset of this period with larger glaciers provided a significant amount of sediments into Lake Bramant and resulted in the formation of a delta that was flooded after AD 1918 (construction of the hydro-electric dam) and that today is found below a water depth of 22 m (Fig. 3). This delta thus attests the onset of a long period of high lake-level with significant glacier activity, in agreement with the studies of Leeman and Niessen (1994), Magny (2004) and Holzhauzer et al. (2005) in the Alpine region. Such a drastic change in Lake Bramant sedimentation after 2850 cal BP is likely due to the onset of the diffluence of the St. Sorlin glacier into the Bramant valley and resulted in an increase in the mean sedimentation rate from 0.59 to 0.67 mm/yr (Fig. 14).

6.2.2. *Interactions of climate conditions and human activity*

Only two terrestrial plant debris were found at the base of core BRA03 in sediments corresponding to the Early Bronze Age and the beginning of the Iron Age (Table 1). The absence of any terrestrial macrofossil material after 2750 cal BP suggests an important change in the vegetation cover at 2500 m a.s.l. (lowering of the tree line) caused by prevailing colder conditions favouring increasing glacier activity in the catchment area.

The copper content anomaly, detected between 483 and 489 cm (Figs. 7 and 14) and dated between 3770 and 3870 cal BP, is most likely reflecting local atmospheric contamination due to mining activity during the Early Bronze Age. This hypothesis is supported by ongoing archaeological investigations in the Grandes Rousses Massif, where evidences of a copper mining industry was recently discovered in the massif, just SE of the catchment area of Lake Bramant and ^{14}C dated around 3800 ± 100 cal BP (Bailly-Maître and Gonon, 2006; Bailly-Maître, oral communication). This mining industry, developed between 2300 and 2650 m a.s.l., likely became possible because of smaller glaciers in the massif in response to a warmer climate during the Early Bronze Age. The fires needed to weaken the rocks for excavating the copper mines (Bailly-Maître, oral communication) were likely alimented with the surrounded vegetation. The change in vegetation cover suggested after 2750 cal BP around Lake Bramant could therefore have also resulted from the interaction of climate change and high-altitude human activities during the Bronze Age.

In addition, the major peaks of heavy metals (especially in lead and copper) dated between AD 115 and 330 and

culminating between AD 130 and 210 are interpreted as resulting from mining activities during the Roman civilization. Lead contamination during the Roman period (100 BC–AD 300) is indeed well documented in various natural archives from the Northern Hemisphere (Hong et al., 1994; Renberg et al., 1994; Shotyk et al., 1998; Boutron et al., 2004). Atmospheric lead contamination shows peaks around AD 128 in the Swiss Jura (Shotyk and Krachler, 2004), around AD 220 in the NW French Alps (Arnaud et al., 2005a b) and around AD 300 in the Mediterranean region (Véron et al., 2006), all marking the Roman civilization apogee.

Presently, no trace of Roman mining activities has been discovered in the Massif. Nevertheless, the identification of lead contamination in Lake Anterne (Fig. 1) and proxies of a local metallurgical activity in the Arve Valley (Arnaud et al., 2005a b) together with the discovery of the lead peak in Lake Bramant sediments suggest an important contamination during the Roman period in the NW Alps around the 2–3rd Centuries. The origin of these important lead contaminations is however still unclear. The origin of Roman land use in the massif (Chardon, 1991) and the growing evidence of mining activities in the Alpine region (Shotyk and Krachler, 2004; Arnaud et al., 2005a b), leading to a strong heavy metal atmospheric contamination in Lake Bramant sediments between AD 130 and 210, may have resulted from a short period of climate change in this part of Europe. This period of mining activity is synchronous with a sharp drop in lake level in the Alpine region at AD ~250 (Magny, 2004) and with small fluctuations of the Great Aletsch glacier in the Swiss Alps between AD 200 and 400 (Holzhauzer et al., 2005). However, no clear changes in glacier activity are observed during this period in the sedimentary record of Lake Bramant. It is therefore suggested that glacier activity above 2500 m a.s.l. in the Grandes Rousses massif may have limited the Roman impact to pasturing and deforestation up to 2000 m a.s.l. in some parts of the massif (cf. Chardon, 1991).

The evolution of the vegetation cover in this part of the massif will be confirmed by ongoing studies of the pollen records in Lake Bramant. Geochemical compositions of these proglacial sediments during the Bronze Age, the Roman period and the Middle Age, together with the identification of the geochemistry of source rocks in the former mines of the Grandes Rousses massif and in the Arve valley, will also be performed to confirm the dominating source areas of atmospheric metallic contamination documented in this study. All together, these data will help disentangling interactions between climate changes and the evolution of high-altitude human activities.

7. Conclusions

This multidisciplinary study of glacial varves from proglacial Lake Bramant is unravelling variations in the amount of fine-grained clastic supply and organic matter, interpreted as changes in glacier activity in the catchment area. The age model originating from an annually resolved record is chiefly supported by radionuclide dating and by the correlation of a large slump with a local earthquake in AD 1881 and of a turbidite with a strong regional earthquake in AD 1822. Natural hazards in this part of the Alps are related to the regional seismicity, but also to the development of exceptional flood deposits that occurred during periods of significant glacier recession.

Glacial varve formation since 4000 years is confirmed by counting laminations between two AMS ^{14}C dates obtained at the base of the core and by the identification of atmospheric metallic contaminations in the sediments, likely resulting from a local and regional mining activity during the Early Bronze-Age and the Roman civilization, respectively.

Two prominent organic-rich intervals, identified on seismic profiles and in the sediment core, were formed during the Bronze Age (4160–3600 and 3300–2850 cal BP) and are probably reflecting periods of reduced glacier activity in the drainage basin, resulting in periods of low-lake level and anoxic conditions. The dramatic lithologic contrast of these two organic-rich units to the remainder of the core reflects the peculiar glacial dynamics with an upstream diffluence that acts as an on–off switch of glacial meltwater supply once a certain climate threshold is reached. The onset of clastic proglacial sedimentation and higher lake level between 3600–3300 cal BP and since 2850 cal BP are reflecting periods of higher glacier activity with meltwater supply into the Bramant Valley. They are synchronous with periods of glacier advances well-documented in the Alps and high-lake levels in west-central Europe.

Evidences for a generally warmer climate during the Bronze Age in this part of the Alps include lowering of the tree line, glacier activity, proglacial lake level and traces of high-altitude mining activities. These reconstructions should however be confirmed by ongoing studies in the evolution of vegetation around the lake and by the identification of the source areas of former mining industry in the western Alps.

Acknowledgements

We would like to thank Michel Vallon (LGGE, Grenoble) and Marie-Christine Bailly-Maître from the Labratoire d'Archéologie Médiévale Méditerranéenne for fruitful scientific discussions. Thanks also to Urs Gerber (ETH Zürich) for the core photographs and to Bruno Axelar (Refuge de l'Etendard) for logistic support and fruitful discussions on Lake Bramant. Pierre Mandaroux and Bertrand Novel (Savoie University) are acknowledged for grain size measurements and varve counting on digital photographs on core BRA03-3, respectively. We would like to sincerely thank Atle Nesje, Oyvind Lie and all the coring team from Bergen University (Norway) for the collection of piston core BRA03 from Lake Bramant and for this

logistic support. Finally, we wish to thank the two anonymous reviewers for their very constructive reviews. This project was funded by the French Mountain Institute. This is GÉOTOP-UQÀM-McGill contribution no. 2007-0050.

References

Allix, A., 1927. Observations glaciologiques faites en Dauphiné jusqu'en 1924, Glacier de Saint Sorlin. Etudes Glaciologiques 6 (Paris, Ministère de l'Agriculture, Direction Générale des Eaux et Forêts, Service d'Etudes des Grandes Forces Hydrauliques. Région des Alpes), 1–26, 30–31, 74–77, 116, 134.

Anselmetti, F.S., Bühler, R., Finger, D., Girardclos, S., Lancini, A., Christian Rellstab, C., Sturm, M., 2007. Effects of Alpine hydropower dams on particle transport and lacustrine sedimentation. Aquatic Sciences 69, 179–198.

Appleby, P.G., Richardson, N., Nolan, P.J., 1991. ^{241}Am dating of lake sediments. Hydrobiologia 214, 35–42.

Arnaud, F., Lignier, V., Revel, M., Desmet, M., Beck, C., Pourchet, M., Charlet, F., Trenteseaux, A., Tribovillard, N., 2002. Dating sediments from an alpine lake (Lake Anterne, NW Alps): influence of flood-events and gravity reworking on ^{210}Pb vertical profile. Terra Nova 14, 225–232.

Arnaud, F., Revel, M., Chapron, E., Desmet, M., Tribovillard, N., 2005a. 7200 years of Rhône river flooding activity in Lake Le Bourget, France: a high resolution sediment record of NW Alps hydrology. The Holocene 15 (3), 420–428.

Arnaud, F., Serralongue, J., Winiarski, T., Desmet, M., Paterne, M., 2005b. Pollution au plomb dans la Savoie antique (II^{e}-III^{e} s. apr. J.-C.) en relation avec une installation métallurgique de la cité de Vienne. Comptes Rendus Geoscience 338, 244–252.

Ariztegui, D., Bianchi, M.M., Masaferro, J., Lafargue, E., Niessen, F., 1997. Interhemispheric synchrony of Late-glacial climatic instability as recorded in proglacial Lake Mascardi, Argentina. Journal of Quaternary Science 12, 333–338.

Bailly-Maitre, M.C., Bruno-Dupraz, J., 1994. Brandes en Oisans: La mine d'argent des Dauphins (XII-XIV e s.) Isère. Documents d'Archéologie en Rhône-Alpes 9, 172.

Bailly-Maître, M.C., Gonon, T., 2006. L'exploitation de la chalcopyrite à l'Âge du Bronze dans le massif des Rousses (Oisans-Isère). In: Proceedings of the 131st Congress of the CTHS. ''Tradition et innovation,'' Grenoble, avril 2006.

Blass, A., Anselmetti, F.S., Ariztegui, D., 2003. 60 years of glaciolacustrine sedimentation in Steinsee (Sustenpass, Switzerland) compared with historic events and instrumental meteorological data: Eclogae. Eclogae Geologicae Helvetiae 96 (Suppl. 1), 59–71.

Blott, S.J., Pye, K., 2001. Gradistat: a grain size distribution and statistics package for the analysis of unconsolided sediments. Earth Surface Processes and Landforms 26, 1237–1248.

Boespflug, X., Long, B.F.N., Occhietti, S., 1995. CAT-Scan in marine stratigraphy: a quantitative approach. Marine Geology 122, 281–301.

Boutron, C., Rosman, K., Barbante, C., Bolshov, M., Adams, F., Hong, S., Ferrari, C., 2004. L'archivage des activités humaines par les neiges et glaces polaires: le cas du plomb. Comptes Rendus Geoscience 336, 847–867.

Brodzikowski, K., Van Loon, A.J., 1991. Review of glacigenic sediments. Development in Sedimentology 49, 688.

Chardon, M., 1991. L'évolution tardiglaciaire et holocène des glaciers et de la végétation autour de l'Alpe d'Huez (Oisans, Alpes Françaises). Revue de Géographie Alpine 2, 39–53.

Chapron, E., Beck, C., Pourchet, M., Deconinck, J-F., 1999. 1822 earthquake-triggered homogenite in Lake Le Bourget (NW Alps). Terra Nova 11, 86–92.

Chapron, E., Desmet, M., De Putter, T., Loutre, M.F., Beck, C., Deconinck, J.F., 2002. Climatic variability in the northwestern Alps, France, as evidenced by 600 years of terrigenous sedimentation in Lake Le Bourget. The Holocene 12 (2), 177–185.

Chapron, E., Arnaud, F., Noël, H., Revel, M., Desmet, M., Perdereau, L., 2005. Rhone River flood deposits in Lake Le Bourget: a proxy for Holocene environmental changes in the NW Alps, France. Boreas 34, 1–13.

Chapron, E., Ariztegui, D., Mulsow, S., Villarosa, G., Pino, M., Outes, V., Juvignié, E., Crivelli, E., 2006. Impact of the 1960 major subduction earthquake in Northern Patagonia. Quaternary International 158, 58–71.

Crémer, J.-F., Long, B., Desrosiers, G., de Montety, L., Locat, J., 2002. Application de la scanographie à l'étude de la densité des sédiments et à la caractérisation des structures sédimentaires: exemple des sédiments déposés dans la rivière Saguenay (Québec, Canada) après la crue de 1996. Canadian Geotechnical Journal 39, 440–450.

Croudace, I.W., Rindby, A., Rothwell, R.G., 2005. ITRAX: description and evaluation of a new X-ray core scanner. In: Rothwell, R.G. (Ed.), New Techniques in Sediment Core Analysis. Geological Society, London, pp. 51–63.

Dahl, S.O., Bakke, J., Lie, O., Nesje, A., 2003. Reconstruction of former glacier equilibrium-line altitudes based on proglacial sites: an evaluation of approaches and selection of sites. Quaternary Science Reviews 22, 275–287.

Deline, P., Orombelli, G., 2005. Glacier fluctuations in the western Alps during the Neoglacial, as indicated by the Miage morainic amphitheatre (Mont Blanc massif, Italy). Boreas 34, 456–467.

Doig, R., 1986. A method for determining the frequency of large-magnitude earthquake using lake sediments. Canadian Journal of Earth Science 23, 930–937.

Edouard, J.L., 1994. Les lacs d'altitude dans les Alpes françaises. Contribution à la connaissance des lacs d'altitude et à l'histoire des milieux montagnards depuis la fin du Tardiglaciaire. Habilitation Thesis, University of Grenoble, 790pp.

Fuselin, G., Jacob, C., Offner, J., 1909. Etudes glaciaires, géographiques et botaniques dans le massif des Grandes Rousses. Etudes glaciologiques, Ministère de l'Agriculture, Paris, pp. 107–112.

Guyard, H., St-Onge, G., Chapron, E., Anselmetti, F., Francus, P., in press. The AD 1881 Earthquake-triggered a slump and late Holocene flood-induced turbidites from proglacial lake Bramant, Western French Alps. In: Lykousis, V., Sakellariou, D., Locat, J. (Eds.), Submarine Mass Movements and their Consequences. Kluwer-Springer.

Holzhauzer, H., Magny, M., Zumbühl, H.J., 2005. Glacier and lake level variations in west-central Europe over the last 3500 years. The Holocene 15 (6), 789–801.

Hong, S., Candelone, J., Patterson, C., Boutron, C., 1994. Greenland ice evidence of hemispheric lead pollution two millennia ago by Greek and Roman civilizations. Science 265, 323–326.

Intergovernmental Panel on Climate Change (IPCC), 2001. Climate Change: Contribution of Working Group I to the Third Assesment Report of the Intergovernmental Panel on Climate Change. Cambridge University Press, New York.

Lamoureux, S.F., Stewart, K.A., Forbes, A.C., Fortin, D., 2006. Multidecadal variations and decline in spring discharge in the Canadian middle Arctic since 1550 AD. Geophysical Research Letters 33, L02403, doi:10.1029/2005GL024942.

Leeman, A., Niessen, F., 1994. Holocene glacial activity and climatic variations in the Swiss Alps: reconstructing a continuous record from proglacial lake sediments. The Holocene 4, 259–268.

Le Meur, E., Vincent, C., 2003. A two-dimensional shallow ice-flow model of Glacier de Saint Sorlin, France. Journal of Glaciology 49, 527–538.

Leonard, E.M., 1997. The relationship between glacial activity and sediment production: evidence from a 4450-year varve record of neoglacial sedimentation in Hector Lake, Alberta, Canada. Journal of Paleolimnology 17, 319–330.

Lliboutry, L., 2002. Extension of Glacier de Saint-Sorlin, Franch Alps and equilibrium-line altitude during the Little Ice Age. Journal of Glaciology 48, 118–124.

Locat, J., Lee, H.J., 2002. Submarine landslides: advances and challenges. Canadian Geotechnical Journal 39, 193–212.

Magny, M., 2004. Holocene climate variability as reflected by mid-European lake-level fluctuations and its probable impact on prehistoric human settlements. Quaternary Internationnal 113, 65–79.

Magny, M., Bégeot, C., Guiot, J., Peyron, O., 2003. Contrasting patterns of hydrological changes in Europe in response to Holocene climate cooling phases. Quaternary Science Reviews 22, 1589–1596.

Matthews, J.A., Karlén, W., 1992. Asynchronous neoglaciation and Holocene climatic change reconstructed from Norwegian glacio-lacustrine sedimentary sequence. Geology 20, 991–994.

Meybeck, M., 1995. Les lacs et leur basin. In: Pouriot, R., Meybeck, M. (Eds.), Limnologie générale. Masson, Paris, pp. 7–59.

Monecke, K., Anselmetti, F., Becker, A., Sturm, M., Giardini, D., 2004. The record of historic earthquakes in lake sediments of Central Switzerland. Tectonophysics 394, 21–40.

Mulder, T., Cochonat, P., 1996. Classification of offshore mass movements. Journal of Sedimentary research 66, 43–57.

Mulder, T., Syvitski, J.P.M., Skene, K.I., 1998. Modelling of erosion and deposition by turbidity currents generated at river mouths. Journal of Sedimetary Research 68, 124–137.

Mulder, T., Migeon, S., Savoye, B., Faugères, J.C., 2001. Inversely graded turbidite sequences in the deep Mediterranean: a record of deposits from flood-generated turbidity currents? Geo-Marine Letters 21, 86–93.

Mulder, T., Syvitski, J.P.M., Migeon, S., Faugères, J-C., Savoye, B., 2003. Marine hyperpycnal flows: initiation, behavior and related deposits. A review. Marine and Petroleum Geology 20, 861–882.

Nesje, A., 1992. A piston corer for lacustrine and marine sediments. Arctic and Alpine Research 24, 257–259.

Nesje, A., Lie, O., Dhal, S.O., 2000. Is the North Atlantic Oscillation reflected in Scandinavian glacier mass balance records? Journal of Quaternary Science 15, 587–601.

Noël, H., Garbolino, E., Brauer, A., Lallier-Vergès, E., de Beaulieu, J.L., Disnar, J.R., 2001. Human impact and soil erosion during the last 5000 yrs as recorded in lacustrine sedimentary organic matter at Lac d'Annecy, the French Alps. Journal of Paleolimnology 25, 229–244.

Nomade, J., Chapron, E., Desmet, M., Reyss, J-L., Arnaud, F., Ligner, V., 2005. Reconstructing historical seismicity from lake sediments (Lake Laffrey, Western Alps, France). Terra Nova 17, 350–357.

Pinglot, J.F., Pourchet, M., 1995. Radioactivity measurements applied to glaciers and lake sediments. The Science of Total Environment 173, 211–223.

Reimer, P.J., Baillie, M.G.L., Bard, E., Bayliss, A., Beck, J.W., Bertrand, C.J.H., Blackwell, P.G., Buck, C.E., Burr, G.S., Cutler, K.B., Damon, P.E., Edwards, R.L., Fairbanks, R.G., Friedrich, M., Guilderson, T.P., Hogg, A.G., Hughen, K.A., Kromer, B., McCormac, F.G., Manning, S.W., Ramsey, C.B., Reimer, R.W., Remmele, S., Southon, J.R., Stuiver, M., Talamo, S., Taylor, F.W., van der Plicht, J., Weyhenmeyer, C.E., 2004. IntCal04 terrestrial radiocarbon age calibration, 26–0 ka BP. Radiocarbon 46, 1029–1058.

Renberg, I., Wik Persson, M., Emteryd, O., 1994. Pre-industrial atmospheric lead contamination detected in Swedish lake sediments. Nature 368, 32–326.

Rothwell, R.G., Hoogakker, B., Thomson, J., Croudace, I.W., Frenz, M., 2006. Turbidite emplacement on the southern Balearic Abyssal Plain (western Mediterranean Sea) during Marine Isotope Stages 1–3: an application of ITRAX XRF scanning of sediment cores to lithostratigraphic analysis. In: Rothwell, R.G. (Ed.), New Techniques in Sediment Core Analysis. Geological Society, London, pp. 79–98.

Schneider, J-L., Pollet, N., Chapron, E., Wessels, M., Wassmer, P., 2004. Signature of Rhine Valley sturzstrom dam failures in Holocene sediments of Lake Constance, Germany. Sedimentary Geology 169, 75–91.

Schnellmann, M., Anselmetti, F., Giardini, D., McKenzie, J.A., 2002. Prehistoric earthquakes history revealed by lacustrine slump deposits. Geology 30, 1131–1134.

Shotyk, W., Krachler, M., 2004. Atmospheric deposition of silver and thallium since 12370 ^{14}C years BP recorded by a Swiss peat bog profile, and comparison with lead and cadmium. Journal of Environmental Monitoring 6, 427–433.

Shotyk, W., Weiss, D., Appleby, P.G., Cheburkin, A.K., Frei, R., Gloor, M., Kramers, J.D., Reese, S., van der Knaap, O., 1998. History of atmospheric lead deposition since 13,370 ^{14}C yr BP recorded in a peat bog profile, Jura Mountains, Switzerland. Science 281, 1635–1640.

Siegenthaler, C., Finger, W., Kelts, K., Wang, W., 1987. Earthquake and seiche deposits in Lake Lucerne, Switzerland. Eclogae Geologicae Helvetiae 80, 241–260.

Six, D., Reynaud, L., Letréguilly, A., 2001. Bilans de masse des glaciers alpins et scandinaves, leurs relations avec l'oscillation du climat de l'Atlantique nord. Earth and Planetary Sciences 333, 693–698.

St-Onge, G., Lajeunesse, P., in press. Flood-induced turbibites from northern Hudson Bay and western Hudson Strait: a two-pulse record of Lake Agassiz final outburst flood? In: Lykousis, V., Sakellariou, D., Locat, J. (Eds.), Submarine Mass Movements and Their Consequences. Kluwer-Springer.

St-Onge, G., Mulder, T., Piper, D.J.W., Hillaire-Marcel, C., Stoner, J.S., 2004. Earthquake and flood induced turbidites on the Saguenay Fjord (Québec): a Holocene paleoseismicity record. Quaternary Science Reviews 23, 283–294.

St-Onge, G., Mulder, T., Francus, P., Long, B., 2007. Continuous physical properties of cored marine sediments. In: Hillaire Marcel, C., de Vernal, A. (Eds.), Proxies in Late Cenozoic Paleoceanography. Elsevier, Amsterdam, pp. 63–98.

Strasser, M., Anselmetti, F., Fäh, D., Giardini, D., Schnellmann, M., 2006. Magnitudes and source areas of large prehistoric northern alpine earthquakes revealed by slope failures in lakes. Geology 34 (12), 1005–1008.

Stuiver, M., Reimer, P.J., Reimer, R.W., 2005. CALIB 5.0. 〈www program and documentation, http://radiocarbon.pa.qub.ac.uk/calib/〉.

Syvitski, J.P.M., Schafer, C.T., 1996. Evidence for an earthquake-triggered basin collapse in Saguenay Fjord, Canada. Sedimentary Geology 104, 127–153.

Syvitski, J.P.M., Vörösmarty, C.J., Kettner, A.J., Green, P., 2005. Impact of humans on the flux of terrestrial sediment to the global coastal ocean. Science 308, 376–380.

Thomas, R.G., Guyodo, Y., Channel, J.E.T., 2003. U-channel track for susceptibility measurements. Geochemistry, Geophysics, Geosystems 4, 6, doi:10.1029/2002GC000454.

Tomkins, J.D., Lamoureux, S.F., 2005. Multiple hydroclimatic controls over recent sedimentation in proglacial Mirror Lake, southern Selwyn Mountains, Northwest Territories. Canadian Journal of Earth Sciences 42, 1589–1599.

Thouvenot, F., Fréchet, J., Jenatton, L., Gamond, J.F., 2003. The Belledonne Border Fault: identification of an active seismic strike-slip fault in the western Alps. Geophysical Journal International 155, 174–192.

Torinesi, O., Letreguilly, A., Valla, F., 2002. A century reconstruction of mass-balance of Glacier de Sarennes, French Alps. Journal of Glaciology 48, 142–148.

Véron, A., Goiran, J.P., Morhange, C., Marriner, N., Empereur, J.Y., 2006. Pollutant lead reveals the pre-Hellenistic occupation and ancient growth of Alexandria, Egypt. Geophysical Research Letters 33, 6, L06409, doi:10.1029/2006GL025824.

Vincent, C., 2002. Influence of climate change over the 20th Century on four French glacier mass balances. Journal of Geophysical Research 107, D19, 4375, doi:10.1029/2001JD000832.

Vörösmarty, C.J., Meybeck, M., Fekete, B., Sharma, K., Green, P., Syvitski, J.P.M., 2003. Anthropogenic sediment retention: major global impact from registered river impoundments. Global and Planetary Change 39 (1–2), 169–190.